Parametric study of cold wire tandem submerged arc welding of heavy gauge X70 linepipe steel

Tailin Ren (tailin@ualberta.ca)
University of Alberta Department of Chemical and Materials Engineering
Mohsen Mohammadijoo
J Barry Wiskel
Robert Lazor
Eric Willett
Douglas G. Ivey
Hani Henein

Research Article

Keywords: Cold wire submerged arc welding, Microalloyed pipeline steel, Taguchi method, Micro-hardness, Weld geometry

Posted Date: March 24th, 2022

DOI: https://doi.org/10.21203/rs.3.rs-1463115/v1

Abstract

Cold wire tandem submerged arc welding (CWTSAW) has been developed to improve the productivity (i.e., deposition rate and travel speed), and to control the weld and heat-affected zone (HAZ) geometry and mechanical properties of heavy gauge pipe. A series of CWTSAW trials were conducted on thick-wall American Petroleum Institute (API) X70 steel plates to investigate the effect of cold wire feed speed (CWFS), heat input (HI) and bevel design (BD) on the resulting geometry (e.g., height of reinforcement area (HRA), bead toe angle (BTA) and coarse grain heat-affected zone (CGHAZ) area) and micro-hardness of the weld and HAZ. The phase fraction of martensite-austenite (MA) constituents was measured using optical microscopy (OM) and scanning electron microscopy (SEM). Vickers micro-hardness measurements were taken of the weld metal and across the HAZ. The geometry and hardness measurements were statistically correlated with the weld parameters using Taguchi methodology. The results showed that the weld bevel design (BD) was the dominant factor influencing the HRA, CGHAZ area and BTA. Cold wire feed speed (CWFS) had a strong influence on the micro-hardness and phase fraction of MA constituents in the CGHAZ.

1.0 Introduction

Submerged arc welding (SAW) is used to produce both UOE and spiral pipe. The trend in pipeline manufacturing is the production of heavier gauge (> 16 mm in wall thickness) X70 pipe. SAW offers substantial benefits, including high deposition rate, deep penetration, and reduced welding times. These attributes are beneficial for welding thick-walled plates [1, 2]. To increase productivity, tandem submerged arc welding (TSAW) containing two or more electrodes has been developed for the welding procedure of line pipe to achieve a high deposition rate [3]. The use of multi-electrode TSAW may, however, result in an increase in overall heat input which affects the metallurgy/properties of the weld metal (WM) and heat-affected zone (HAZ), especially in the coarse grain heat affected zone (CGHAZ). Consequently, the quality of weldments, such as toughness and microstructure, may deteriorate [4, 5]. To increase productivity while maintaining the quality of TSAW pipeline products, cold wire tandem submerged arc welding (CWTSAW) was developed [6, 7].

CWTSAW is defined as a TSAW process where an additional electrode with no arc is introduced within the molten pool. The primary objective of involving a cold wire is to increase the deposition rate and decrease the overall heat input into the weld. This method was first developed by Mruczek et al. [6] in the SAW process for enhancing welding capabilities and improving weld productivity by increasing deposition rate. Mohammadijoo et al. [7] applied cold wire addition to the TSAW process of an intermediate thickness X70 line pipe (13.4 mm). The cold wire was placed at a lagging position next to the trailing electrode where it consumed heat from the weld pool. In addition, placing the cold wire at a lagging position angle of 63° resulted in an overall improvement in the weld geometry and mechanical properties. This work showed a decrease in overall heat input, an increase in deposition rate and enhanced productivity of X70 line pipe welding. Ramakrishnan et al. [8–10] has published several studies related to cold wire addition. For instance, the CGHAZ of butt welds in pressure vessel applications is reduced by 30% as compared with conventional SAW due to the cold wire addition, and the cold wire technique leads to 40% reduction in the number of passes and a 30% saving in flux consumption [8]. Multiple wires (three or four wires) and cold wire addition are utilized in SAW welds and these contribute to a higher deposition rate and improved toughness relative to conventional weldments [9]. In addition, the fracture toughness in the narrow groove SAW process is improved due to the low heat input of the cold wire addition [10].

The Taguchi method is a statistical technique used to analyze and optimize manufacturing processes [11]. This method has been used in numerous studies to optimize the welding process. Tarng et al. [12] determined the optimal welding parameters of the SAW process with a small number of tests utilizing Taguchi analysis. Sarkar et al. [13] employed Taguchi techniques to analyze the effective contribution of bead geometry on tensile strength and validated the results with confirmatory tests in the SAW process. In addition, Mohammadijoo et al. [7] employed the Taguchi method to optimize the CWTSAW process of intermediate gauge X70 steels by defining significant welding parameters and suitable levels of process parameters.

In this study, the CWTSAW process was applied to heavy gauge (19.1 mm thick) X70 line pipe steel. The effects of heat input of the lead (HIL) and trail (HIT) electrodes, voltage of the lead (VL) and trail (VT) electrodes, travel speed (TS), bevel design (BD), and cold wire feed speed (CWFS) on the weld geometry, hardness of the HAZ and microstructural modification in the CGHAZ were studied. In total, 16 test welds were conducted. The specific test welds were designed using the Taguchi method. Following welding, the weld geometrical characteristics were measured including the reinforcement area (RA), the height of the reinforcement area (HRA), bead

toe angle (BTA), aspect ratio (AR), semi-penetration ratio (SPR), and coarse grain heat-affected zone (CGHAZ) area. In addition, the amount of weld dilution (DIL) and the micro-hardness of the CGHAZ and WM were measured.

The measurements were analyzed using three statistical methods; i.e., analysis of variance (ANOVA), three order multiple regression (TOMR) analysis ,and signal-to-noise (S/N) ratio. ANOVA was used to determine the significant weld parameters by analyzing the variability of the data using the variance ratio (F value), sum of squares (SS), and level of significance (P value) [14]. TOMR analysis is a nonlinear model used to develop empirical equations for response characteristics and mechanical properties, such as the SPR, RA, HRA, CGHAZ area, and micro-hardness of the CGHAZ and WM [15]. S/N ratio is the method for optimizing the levels of weld parameters to improve weld geometry [16]. Finally, a comparison of martensite-austenite (MA) constituents in the CGHAZ of the conventional TSAW and CWTSAW processes was undertaken using optical microscopy (OM) and scanning electron microscopy (SEM).

2.0 Experimental Methods

2.1 Base and Electrode Material

The CWTSAW weld tests were conducted on heavy gauge (19.1 mm thick) X70 microalloyed steel. The composition of the X70 steel is shown in Table 1. The studied X70 microalloyed steel was fabricated by Evraz Inc. NA through thermo-mechanical controlled processing (TMCP) [2].

The electrodes used in the study for both hot wires and the cold wire were BA-S2Mo, Bavaria (EN756/EN14298). A 4 mm diameter BA-S2Mo solid wire was selected for the electrodes and cold wire. The composition is shown in Table 1.

2.2 Weld Bevel Specifications

Weld samples were fabricated and machined with two different bevel designs. Figure 1 compares the two bevel types used. Each bevel is generated on the same thickness of weld skelp, but the cross-sectional areas are different. For instance, the 60° bevel with a 4.5 mm depth has a 12 mm^2 cross-sectional area, while the 90° bevel with a 5 mm depth has a larger cross-sectional area of 25 mm^2. The quantitative description of the bevel specification is convenient for the representation of the two bevel types in statistical analysis.

2.3 CWTSAW Setup

Three electrodes (lead, trail and cold electrode) were fed into the molten pool, as illustrated in Fig. 2a. The electrically cold electrode is located at a lagging position relative to the trail electrode. The electrode setup is shown in Fig. 2b, including the stick out length (25 mm), electrode separation (13 mm) and the angular position of each electrode relative to a normal to the skelp surface. The constant power source of the lead and trail electrodes were direct current electrode positive (DCEP) polarity and square wave alternating current (ACSQ) polarity, respectively. There was no power source for the cold electrode. As a basic feature in SAW, a consumable granular flux is needed to shield the welding pool and to fill the bevel area. BF6.5 consumable flux produced by Bavaria in Germany, according to EN 760, was used in the CWTSAW process.

2.4 Welding Parameters

The four fundamental welding parameters are current, voltage, travel speed, and feed speed of the electrodes. For the CWTSAW process, there are additional welding parameters based on the use of multiple electrodes. However, in order to understand the effect of heat input on the weldments and to keep the number of welding tests manageable, the current of the lead and trail electrodes was not varied independently and the feed speed of the trail and lead electrodes was kept constant. The nominal heat input (HI) and voltage (V) are key welding parameters and the current was calculated and set during welding according to Eq. 1 [7].

$$\mathrm{HI}\left(\frac{\mathrm{kJ}}{\mathrm{mm}}\right) = \frac{\square \bullet \mathrm{V} \bullet \mathrm{I}}{1000 \bullet \mathrm{TS}}$$

1

Where HI, V, I and TS represent nominal heat input, voltage, current, and travel speed. The arc efficiency ($\square$) is the range of 0.9-1.0 for SAW [7].

Seven welding parameters with mixed levels, including five main welding parameters such as heat input and voltage of lead and trail electrodes and travel speed, were selected for CWTSAW tests. These are shown in Table 2. The heat input, voltage, and travel speed are fundamental and crucial parameters for a welding process and need to be included. Moreover, the cold wire parameter and bevel specification parameter are CWFS and BD, respectively. CWFS and BD were selected to study the effect of the cold wire addition and varied bevel types on weld characteristics and hardness. Only CWFS is a four-level welding parameter and the others are two-level.

2.5 Experimental Table

Taguchi analysis was employed for the parametric study of CWTSAW. The main advantage of Taguchi analysis is the use of a small number of welding tests, which is more economical and effective than using a factorial design [11]. Based on six parameters with two levels and one parameter with four levels, an L16 orthogonal array (OA) was designed using Taguchi analysis and is shown in Table 3. The L16 array comprised 16 weld tests and each level of the parameters appears the same number of times in each column. The weld geometrical values were measured for all 16 weld tests and analyzed using statistical methods. Additionally, a welding table of three validation tests is shown in Table 4. These tests were used to validate the linear trend between the measured and predicted results in the TOMR analysis.

2.6 Weld Characteristics

Three weld samples extracted from each weldment, as shown in Fig. 3a, were used to measure geometry characteristics. A total of 48 specimens was examined. Each sample was mounted and polished following the ASTM E3-11 standard [17] and then were macro-etched using 4% Nital to reveal the HAZ and WM boundaries (Fig. 3b). A stereomicroscope image was obtained from each section and analyzed using Image J to obtain the weld geometry values, including bead width (BW), penetration depth (PD), penetration area (PA), bead width at half penetration depth ($BW_{1/2}$), HRA, RA, bead toe angle (BTA), and CGHAZ area as per Fig. 3b.

The weld geometry values obtained from the stereomicroscope images were utilized to calculate AR, SPR, and the amount of DIL of the weld, as shown in Equations 2 to 4, respectively.

$$AR = \frac{\mathrm{PD}}{\mathrm{BW}} \quad (2)$$

$$SPR = \frac{BW_{1/2}}{\mathrm{BW}} \quad (3)$$

$$DIL = \frac{\mathrm{PA} - \mathrm{bevelarea}}{\mathrm{PA} + \mathrm{RA}} \quad (4)$$

The bevel areas in the two bevel specifications were 12 mm^2 and 25 mm^2 (Fig. 1).

2.7 Micro-hardness

Vickers micro-hardness measurements were obtained from the BM, HAZ and WM, as illustrated in Fig. 4 [18]. Two indentation lines (5 mm below the surface) contained a total of 50 indents from each weld sample to guarantee 10 to 12 indents in the WM and CGHAZ. A 500 g load and a dwell time of 14 s were used. The distance between two indents was three times the size of an indent, as indicated in the optical images in Fig. 4.

2.8 Microstructural Characterization

Optical microscopy (OM) was conducted using an Olympus BX61 microscope and Olympus StreamMotion software. Scanning electron microscopy (SEM) was done using a Zeiss EVO M10 SEM operating at 20 kV accelerating voltage. The weld specimens were micro-etched with modified LePera's solution to reveal MA constituents in the HAZ [19]. Then, three optical and three SEM second electron (SE) micrographs were taken from a location 5 mm below the weld surface and 50–200 µm from the fusion line. The phase

fractions of MA constituents in the CGHAZ of TSAW and CWTSAW welds were measured from both optical and SEM micrographs using the color threshold feature of Image J 1.52a software.

3.0 Results

The BW, HRA, BTA, RA, CGHAZ area, CGHAZ hardness, WM hardness, PA, PD, and $BW_{1/2}$ were measured for all 16 test welds. The values for each characteristic are shown in Table 5. Of particular note is the largest value of CGHAZA (30.2 mm^2) observed for Test 8. This test had the highest heat input of all the welds. Maximum values for other characteristics are indicated in bold and minimum values are underlined in each column.

The calculated values for AR, SPR, and DIL are shown in Table 6. Maximum values for each calculated characteristic are indicated in bold and minimum values are underlined in each column. The largest values of AR and SPR are for Test 8 (highest heat input). The lowest amount of DIL is observed in Test 13. In general, a lower amount of DIL leads to better weld properties, as reported in references [20, 21].

The relationship between different weld characteristics can be made to help understand the welding process. Figure 5a shows a plot of PA vs. CGHAZ area, where CGHAZ area is shown to increase as PA increases. The trend line shown is for illustrative purposes only. This indicates that as weld metal size increases (via heat input and bevel design) an accompanying increase in CGHAZ area will occur. Both Test 4 and Test 8 appear to show significant increases in PA relative to the size of the CGHAZ area. Test 8 has the highest heat input and Test 4 appears to be an outlier.

The relationship between RA and CGHAZ area is shown in Fig. 5b. The CGHAZ area increases as RA decreases. The decreased RA may facilitate full penetration in the weld which may influence the size of the CGHAZ area. The bevel design (BD) is also believed to influence the observed correlation between the RA and CGHAZ area. This will be discussed in Section 4.1. Additional analysis of the correlation between welding parameters and measured weld geometry is presented in Section 4.2.

4.0 Discussion

4.1 Significance of Welding Parameters

The analysis of variance (ANOVA) was carried out on the measured weld characteristics to determine the statistical significance of the welding parameters. All ANOVA tables are presented in Appendix A (Table 10) and include probabilities of significance (P), degrees of freedom (DOF), sum of squares (SS), variance ratios (F), and R^2 values for each welding parameter. According to the statistical analysis reported by Mruczek et al. [6] and Shahverdi et al. [22], P values are used to determine the statistical significance of each of the welding parameters. A P value equal to or less than 0.05 indicates the parameter is statistically significant with 95% confidence. A P value of 0.25 corresponds to a 75% confidence level that the parameter is statistically significant for the weld characteristic. The P values for individual weld geometry results and micro-hardness values for the CGHAZ and WM are listed in Table 7, along with confidence levels. For 95% and 75% confidence levels, the significant welding parameters are highlighed in bold. For example, the significant welding parameters affecting reinforcement area (RA) are heat input of the trail electrode (HIT), voltage of the trail electode (VT) and bevel design (BD), all with a confidence level of 95%.

The effective contribution of each parameter depends on the sum of squares, which is the deviation from the total average value of population. The concept of the effective contribution is a fundamental term in ANOVA analysis and can be calculated by Eq. 5 [14].

$$\%\ = \frac{SS_i}{SS_t} \bullet 100\%$$

5

where is the effective contribution of each parameter to the response characteristics and SS_i and SS_t are the sum of squares for each parameter and the total sum of squares, respectively. The contribution evaluates the importance of parameters on each weld characteristic and the WM and CGHAZ micro-hardness. The significant contributions for BW, AR, DIL, and SPR are shown in Fig. 6.

Overall voltage (lead + trail electrodes) and TS significantly influence BW, AR, and SPR, as shown in Fig. 6. It is generally accepted that a higher arc voltage leads to a wider arc length promoting the formation of a wide BW [23]–[25]. Thomas et al. [26] correlated TS with BW of heavy gauge strip and reported that a high TS reduces the filler metal per unit length of weld leading to a narrow weld. Specifically, a faster TS and lower V result in a shorter arc length and, as such, a smaller BW. The AR and SPR were calculated using Equations 2 and 3. Both geometric ratio results are significantly affected by VL and TS. An increasing TS results in a smaller BW due to the reduced heat input and reduced melted metal per unit length [25, 27]. Therefore, both AR and SPR are affected by voltage and TS, due to the change in BW. Dilution is defined as the ratio of the amount of adjacent metal melted to the total amount of fused metal. The amount of dilution is affected by two geometric results, PA and RA, as expressed in Eq. 4. There are two significant parameters, HIL and VT, that affect PA and RA. In this study, the polarity of the HIL is DCEP in the welding process producing a weld with good penetration [25, 28]. Therefore, a higher HIL increases the penetration depth leading to more dilution. Finally, it is common to minimize the amount of dilution since the amount of dilution affects the composition of the molten pool and the resultant mechanical properties in the welds [7, 29].

Figure 7 shows that the CWFS has the most dominant effect on the CGHAZ and WM micro-hardness profiles, since cold wire addition alters the local thermal cycle by absorbing the heat from the molten pool. Mohammadijoo et al. [30, 31] evaluated the effect of cold wire addition on heat input and hardness profile in the HAZ and they reported that increasing the CWFS leads to a higher hardness because of the faster cooling rate. In addition, the heat input and voltage may also contribute to the CGHAZ hardness profile since they can change the local thermal cycle and the size of the CGHAZ area. It is difficult to compare the effects of CWFS on hardness when other parameters are varied as well. Therefore, nonlinear relationship analysis between interactions of welding parameters and micro-hardness profiles in the CGHAZ and WM is necessary and is discussed in Subsection 4.2.

In Fig. 8, BD had the greatest effect on HRA, BTA, CGHAZ area, and RA. In order to understand the effect of BD, the 16 measurements of RA, HRA, BTA, and CGHAZ area were plotted against two bevel specifications separately, as shown in Fig. 9. The BD with a wider bevel area had lower RA and HRA, and increased BTA and CGHAZ area. This means that smaller and shallower reinforcement regions were produced for the larger bevel angle.

According to the study on the influence of bevel angle on heat transfer and fluid flow in the welding pool, published by Chen et al. [32], increasing the bevel angle from 60° to 90° resulted in more liquid metal flowing downward. This means that increased bevel angle promotes heat transfer from the top to the bottom of the weld leading to full penetration. Huang et al. [33] also studied the effect of groove angle on weld depth in tungsten inert gas (TIG) welding by analyzing the current density and arc pressure. When the groove angle was increased, the current density and arc pressure were elevated at the groove bottom position, because of the concentrated arc heat input and stronger electromagnetic force at the bottom region of the high groove angle in comparison to the low groove angle [33]. This phenomenon indicates that there is a smaller RA in the wider BD than the shallower BD due to the achievement of full penetration.

The formation of a larger CGHAZ area in the deep BD than in the shallow BD is supported by Chen's simulation study of thermal cycles in the molten pool. The finding showed that the width of the overheated zone (1100°C – 1500°C) increased when the bevel angle changed from 60° to 90°, which promoted the formation of a coarse grain structure. The reason for this phenomenon is that the arc and molten metal contacted a larger area when the bevel angle was larger, so that the solid metal phase easily conducted more heat to expand the overheated zone [32].

The BD had a smaller effect on the weld geometry (SPR and AR) and dilution than HI, V and TS, as shown in Fig. 6. The values of SPR and AR were calculated from the BW. The smaller effect of BD on the BW can be explained in terms of the main liquid metal flow pattern and surface tension in the molten pool. The main flow pattern of liquid metal in the molten pool is liquid metal flowing upward along the boundary of the molten pool and colliding at the top of the weld, whereupon the liquid metal changes direction and descends into the pool [32].

The main flow pattern of liquid metal and surface tension are governed the BW and they are affected by active elements, such as O, S, Si, and Ni, dissolved in the liquid mixture metal [32, 34]. The BW is controlled by the surface tension force since it pulls liquid metal towards the center of the weld pool, which is varied by the concentration of the active elements. Another study reported that bead width depends on the concentration of surface active elements and the local temperature profile [35]. In this study, the composition of the base metal X70 steel, the electrodes, and the granular flux were uniform and identical for all 16 fabricated weldments. This

means that the main flow pattern, surface tension, and BW were not altered even for different bevel angles and bevel depths. Therefore, the BD had little influence on the weld geometry ratio.

4.2 Nonlinear Relationship of CWTSAW

Three order multiple regression (TOMR) was used to analyze the nonlinear relationship of controllable variables and the response factors. The empirical equations were developed using Minitab 18 with the form in Eq. 6.

$$y = C_0 + \sum_{i=1}^{7}\left(C_i \bullet x_i\right) + \sum_{i=1}^{7}\left(C_{ii} \bullet x_i^2\right) + \sum_{i=1}^{7}\sum_{i>j}^{7}\left(C_{ij} \bullet x_i \bullet x_j\right) + \sum_{i=1}^{7}\left(C_{iii} \bullet x_i^3\right) + \sum_{i=1}^{7}\sum_{j>i}^{7}\sum_{k>j}^{7}\left(C_{ijk} \bullet x_i \bullet x_j \bullet x_k\right)$$

6

where y is the response factor (geometry characteristics and micro-hardness profile) which was predicted by the controllable variable x_i(welding parameters and different interactive combinations); C_i, C_{ii}, C_{ij}, C_{iii}, and C_{ijk} are the coefficients. In this study, the confidence level of TOMR in Minitab 18 was set at 90% which means that any controllable variables with a P value less than or equal to 0.1 are statistically significant and considered as predictors in empirical equations. For example, 8 predictors in the CGHAZ micro-hardness TOMR equation from a total of 72 possible predictors (individual welding parameters and interactions) were considered which resulted in a good fit.

CGHAZ micro-hardness = 112 + 1.86• CWFS + 298• HIL − 13.31• VL + 1.44• TS -0.0327• $CWFS^2$-5.89• HIL• TS + 0.264• VL• TS + 0.000169• $CWFS^3$ (7)

Of particular note is that squared and cubed predictors are only associated with CWFS in the CGHAZ micro-hardness equation. This appears to be the dominant effect contributed by cold wire addition in comparison with other TOMR equations. The other TOMR equations for HRA, RA, CGHAZ area, SPR, and WM micro-hardness are shown in Appendix A.

The calculated values for HRA, RA, CGHAZ area, micro-hardness of the CGHAZ, and WM are plotted against the observed values in Fig. 10. To validate each equation, three (3) complementary tests were conducted and are included in Fig. 10 (triangles). The weld table for these complementary tests is shown in Table 4. Overall, the range of R^2 values is from 81.6–97.9% and the geometric characteristics of the three complementary tests with the varied welding parameters levels show good correlation with the observed values (Fig. 10).

4.3 Optimized Levels of CWTSAW

The S/N ratio was utilized to determine the optimized levels for each welding parameter. The welding parameters were categorized by two quality requirements, which are “lower-the-better” and “higher-the-better”, respectively. AR, BTA, APR, and BW are included in the “higher-the-better” quality requirements. DIL, CGHAZ area, HRA, and RA are included in the “lower-the-better” quality requirements. The S/N ratio analysis was not conducted on the micro-hardness profiles since there is not agreement on which approach is better. The S/N ratio was calculated using Equations 8 and 9 [16].

$$\eta_{(\mathrm{lower-the-bettter})} = -10\log_{10}\left(\frac{1}{n}\sum_{i=1}^{n} y_{ij}^2\right)$$

8

$$\eta_{(\mathrm{higher-the-bettter})} = -10\log_{10}\left(\frac{1}{n}\sum_{i=1}^{n}\frac{1}{y_{ij}^2}\right)$$

9

where η is the S/N value, y_{ij} is the experimental value of the ith response characteristic in the jth test, and n is the number of tests.

A higher average S/N ratio value representing a given level of the weld parameter resulted in an optimal effect on the geometric characteristics, since higher S/N values mean lower noise effects [15, 36]. A weld parameter level with a higher S/N value is considered as the optimized parameter level, which results in an optimal effect on the geometric characteristics. The calculated S/N ratio values for the weld characteristics are shown in Appendix A (Table 11). Based on the calculated S/N ratio values, the optimized levels for the CWTSAW parameters are summarized (Table 8). Overall, the optimal geometric characteristics are achieved using optimized levels of CWTSAW parameters; i.e., 1.6 kJ/mm for HIL (level 1), 1.3 kJ/mm for HIT (level 1), 21.2 mm/s for TS (level 1), and 25mm^2 for BD (level 2).

4.4 Comparison of TSAW and CWTSAW

Two heavy gauge X70 welds were produced by conventional tandem submerged arc welding (TSAW) and cold wire TSAW (CWTSAW) processes. Then, a comparison in terms of average micro-hardness and the phase fraction of MA constituents in the CGHAZ of TSAW and CWTSAW weld was undertaken. The weld testing conditions are shown in Table 9. The HIL, HIT, VL, VT, TS ,and BD for both the TSAW and CWTSAW weld are identical and only the CWFS is varied.

The strategy of micro-hardness measurement followed the schematic description in Fig. 4. Figure 11 shows that the average micro-hardness values measured in the CGHAZ of the TSAW and CWTSAW welds. The hardness is higher for the CGHAZ of the TSAW weld than for the CWTSAW weld. The lower hardness distribution in the CGHAZ of CWTSAW weld is closely related to the microstructure modification due to heat reduction by heat consumption of the cold wire addition.

Optical and SEM SE micrographs of MA constituents in the CGHAZ of TSAW and CWTSAW samples are shown in Fig. 12. The MA constituents appear as shiny white features in the optical and SEM images after etching with the modified LePera's etchant [19]. White linear segments are visible in the SEM images, since some of the MA constituents were formed at the grain boundaries (Fig. 12b and d). The MA fractions from the optical micrographs (Fig. 12a and b) are 5.3% (0.2%) and 2.8% (0.1%) for the TSAW and CWTSAW welds, respectively. The MA fractions in the CGHAZ determined from the SEM micrographs are 5.7% (0.2%) and 3.3% (0.2%) for TSAW and CWTSAW samples, respectively. The values in the brackets are one standard deviation. The trend for the MA phase fraction in the CGHAZ for both welds is consistent. In terms of the morphology of MA constituents, the MA regions in the TSAW sample from both optical and SEM SE micrographs are mainly massive and the MA constituents of the TSAW sample are more elongated and larger than those in the CWTSAW sample. The MA features in the CWTSAW sample are finer and more dispersed than those in the TSAW sample.

The CWTSAW samples have lower MA fractions with fine and dispersed MA constituents (Fig. 12c and d). The average micro-hardness in the CGHAZ of TSAW samples is higher than that in the CWTSAW sample, which can be correlated with the higher MA volume fraction and the different MA morphology (blocky and elongated) in the TSAW sample. Luo et al. [37] and Mohammadijoo et al. [38, 39] analyzed the morphology of martensite-austenite (MA) constituents in the CGHAZ with respect to the fracture toughness. They reported similar findings that denser MA regions with elongated MA constituents were formed at prior austenite grain (PAG) boundaries, which resulted in localized brittle zones (LBZs). The formation of LBZs can cause initiation and propagation of cleavage fracture at the PAG boundaries in the HAZ, deteriorating the fracture toughness. There are elongated MA constituents and a higher overall MA fraction in the CGHAZ of the TSAW sample than in the CWTSAW sample. This can be interpreted as the reason for the higher hardness in the CGHAZ of the TSAW samples.

5.0 Conclusions

The influence of cold wire addition in CWTSAW on weld geometry and micro-hardness profiles of the coarse grain heat-affected zone (CGHAZ) in heavy gauge (19.1 mm thick) X70 steels has been studied and optimized parametrically. The following general conclusions can be made:

- The voltage of the lead and trail electrodes had a significant effect on the bead width, penetration profile, and reinforcement shape. Higher voltage resulted in increased bead width and bead toe angle. Higher lead electrode voltage resulted in decreased CGHAZ area, aspect ratio, and semi-penetration ratio.
- Cold wire feed speed had a secondary effect on the height of reinforcement area. An increase in cold wire feed speed resulted in a lower height of reinforcement area.

- Bevel design had a significant effect on the height of reinforcement area, reinforcement area, bead toe angle, and CGHAZ area, but only a minor effect on the weld metal and CGHAZ micro-hardness.
- Cold wire feed speed had the most dominant effect on the weld metal and CGHAZ micro-hardness profiles, since the cold wire addition altered the local thermal cycle by consuming heat from the molten pool.
- A cold wire tandem submerged arc welding process, with a heat input for the lead electrode of 1.3 kJ/mm, a heat input for the trail electrode of 1.6 kJ/mm, a travel speed of 21.2 mm/s, a bevel angle of 90°, and a bevel depth of 5 mm reduced the CGHAZ area, dilution, height of reinforcement area, and reinforcement area and increased bead width, penetration depth and bead toe angle.

Declarations

Acknowledgments

The authors would like to acknowledge the Natural Sciences and Engineering Research Council (NSERC) of Canada, Evraz Inc. NA and TC Energy Corp. for providing financial support. Special thanks are also in order for the Research and Development Division of Evraz Inc. NA for providing welding equipment and technical assistance to conduct welding tests.

Data availability All data generated or analyzed during this study are included in this published article.

Code availability Not applicable

Funding This research was financially supported by the Natural Sciences and Engineering Research Council (NSERC) of Canada, Evraz Inc. NA and TC Energy Corp.

Ethics approval Not applicable.

Consent to participate Not applicable.

Consent for publication Not applicable.

Conflict of interest The authors declare no competing interests.

References

1. Weman K (2012) Welding Processes Handbook (2nd Edition) - Knovel. Woodhead Publishing
2. Collins LE, Dunnett K, Hylton T, Ray A (2018) “Development of heavy gauge X70 helical line pipe,” *Proc. Bienn. Int. Pipeline Conf. IPC*, vol. 3, pp. 1–9,
3. Bortsov AN, Shabalov IP, Velichko AA, Mentyukov KY, Utkin IY (2013) Features of multi-electrode submerged-arc welding in the production of high-strength thick-walled pipes. Metallurgist 57:3–4
4. Moeinifar S, Kokabi AH, Madaah Hosseini HR, Shang CJ, Hui G, Wei LZ (2015) “Influence of four wires tandem submerged arc welding process on heat affected zone properties in high strength pipeline steel,” *Proc. 2010 Int. Conf. Mech. Ind. Manuf. Technol. MIMT 2010*, no. April pp. 85–89, 2010
5. Far SM (2012) “Influence of thermal simulated and real tandem submerged arc welding process on the microstructure and mechanical properties of the coarse grained heat affected zone,”Appl. Mech. Mater., vol.110–116, pp. 3191–3198,
6. Mruczek MF, Parker D (2006) “Cold Wire Feed Submerged Arc Welding,” Johnstown, PA,
7. Mohammadijoo M, Kenny S, Collins L, Henein H, Ivey DG (2017) “Influence of cold-wire tandem submerged arc welding parameters on weld geometry and microhardness of microalloyed pipeline steels,”Int. J. Adv. Manuf. Technol., pp.2249–2263,
8. Ramakrishnan M, Muthupandi V (2012) Application of submerged arc welding technology with cold wire addition for drum shell long seam butt welds of pressure vessel components. Int J Adv Manuf Technol 65:5–8
9. Ramakrishnan SKJ, Mannarsamy* SK, PiyushThakor* (2015) Gautam Chauhan* and and R. korada Korada*, “Establishment of cold wire addition technology in multiwire submerged arc welding for line pipe manufacturing to improve the weldment quality,” *ASME 2015 India Oil Gas Pipeline Conf.*, pp. 1–11,

10. Ramakrishnan M, Padmanaban K, Muthupandi V (2013) Studies on fracture toughness of cold wire addition in narrow groove submerged arc welding process. Int J Adv Manuf Technol 68:1–4
11. Taguchi G (1993) Taguchi on Robust Technology Development: Bringing Quality Engineering Upstream. ASME Press
12. Tarng YS, Yang WH (1998) Application of the Taguchi method to the optimization of the submerged arc welding process. Mater Manuf Process 13(3):455–467
13. Sarkar A, Roy J, Majumder A, Saha SC (2014) Optimization of Welding Parameters of Submerged Arc Welding Using Analytic Hierarchy Process (AHP) Based on Taguchi Technique. J Inst Eng Ser C 95(2):159–168
14. Roy RK, Primer on the Taguchi Method (2010) " (2nd Edition) – 6. Analysis of Variance (ANOVA)," in *Primer on the Taguchi Method*, 2nd ed., R. K. Roy, Ed. Society of Manufacturing Engineers (SME),
15. Mathews PG (2005) Design of Experiments with MINITAB. In: Mathews PG (ed) " in Linear Regression. American Society for Quality (ASQ), pp 273–346
16. Mason RL, Gunst RF, Hess JL (2003) "Analysis of Nested Designs and Designs for Process Improvement," in *Statistical Design and Analysis of Experiments - With Applications to Engineering and Science*, 2nd Editio., vol. 1, pp. 423–458
17. International ASTM (2017) "ASTM E3-11 Stardard Guide for Preparation of metallographic specimens," *ASTM Stand.*, vol. 11, no. Reapproved pp. 1–17, 2017
18. ASTM E384–17 (2017) "Standard Test Method for Microindentation Hardness of Materials,"ASTM Int., pp.1–40,
19. Mohammadijoo M, Henein H, Ivey DG, "MICROSTRUCTURAL CHARACTERIZATION OF THE HAZ IN WELDED (2016)," in *Microscopy Society of Canada 2016 MSC/SMC 43rd Annual Meeting*, no. July, pp. 2–4
20. Reisgen U, Dilthey U, Aretov I (2008) "SAW cold wire technology - Economic alternative for joining hot crack sensitive nickel-base alloys,"Hot Crack. Phenom. Welds II, pp.215–237,
21. Murugan N, Parmar RS, Sud SK (1993) Effect of submerged arc process variables on dilution and bead geometry in single wire surfacing. J Mater Process Tech 37:1–4
22. Shahverdi Shahraki H, Mozafari H (2015) Modeling and Optimizing of Submerged Arc Welding Process by Taguchi Design of Experiments in Presence of Magnesium Oxide Nano-Particles. Appl Mech Mater 763:52–57
23. O'Brien A, Handbook "Welding (2004) Volume 2 - Welding Processes, Part 1–6.5 Process variables," 9th Editio., American Welding Society (AWS), pp. 278–282
24. Weman K (2012) "10.4.2 Welding Parameters and Weld Quality," in *Welding Processes Handbook (2nd Edition)*, 2nd ed., Woodhead Publishing, pp. 113–114
25. Pepin J, Penniston C, Henein H, Ivey DG, Collins L, Boyd D (2012) Using semipenetration ratio to characterize effects of waveform variables on bead profile and heat affected zone with single electrode submerged arc welding. Can Metall Q 51(3):284–293
26. Cary H (1993) Weld Overlays, Welding, Brazing, and Soldering, vol 6. American Society for Metals International
27. O'Brien A (2004) "6.5 Process Variables," in *Welding Handbook, Volume 2 - Welding Processes, Part 1*, 9th Editio., American Welding Society (AWS), pp. 278–282
28. Singh RP, Garg RK, Shukla DK (2016) Mathematical modeling of effect of polarity on weld bead geometry in submerged arc welding. J Manuf Process 21:14–22
29. Sun MKz (2020) "High Productivity Cladding with Non-Consumable Electrode Arc Processes," in *6'th International Trendsin Welding Research Conference Proceedings*, no. April 2002, pp. 15–19
30. Mohammadijoo M, Collins L, Henein H, Ivey DG (2017) Evaluation of cold wire addition effect on heat input and productivity of tandem submerged arc welding for low-carbon microalloyed steels. Int J Adv Manuf Technol 92:1–4
31. Mohammadijoo M, Kenny S, Collins L, Henein H, Ivey DG (2017) Characterization of HAZ of API X70 Microalloyed Steel Welded by Cold-Wire Tandem Submerged Arc Welding. Metall Mater Trans A Phys Metall Mater Sci 48(5):2247–2259
32. Chen J, Schwenk C, Wu CS, Rethmeier M (2012) Predicting the influence of groove angle on heat transfer and fluid flow for new gas metal arc welding processes. Int J Heat Mass Transf 55:1–3
33. Huang Y, Yu H, Zhang J, Ren C (2019) Study on arc physical characteristics of GPCA-TIG welding under different angles of V groove. Eng Res Express 1(1):015032

34. Ribic B, Tsukamoto S, Rai R, DebRoy T (2011) “Role of surface-active elements during keyhole-mode laser welding,”J. Phys. D. Appl. Phys., vol. 44, no. 48,
35. Kannan PR, Muthupandi V, Devakumaran K (2018) “On the effect of temperature coefficient of surface tension on shape and geometry of weld beads in hot wire gas tungsten arc welding process,” *Mater. Today Proc.*, vol. 5, no. 2, pp. 7845–7852,
36. Gowthaman K, Saiganesh J, Rajamanikam CS (2013) “Determination of submerged arc welding process parameters using Taguchi method and regression analysis,” *2013 Int. Conf. Energy Effic. Technol. Sustain. ICEETS* pp. 842–847, 2013
37. Luo X, Chen X, Wang T, Pan S, Wang Z (2017) “Effect of morphologies of martensite–austenite constituents on impact toughness in intercritically reheated coarse-grained heat-affected zone of HSLA steel,” *Mater. Sci. Eng. A*, vol. 710, no. October pp. 192–199, 2018
38. Mohammadijoo M, Collins L, Lazor R, Henein H, Ivey DG (2018) “Influence of Cold-Wire Submerged Arc Welding on the Toughness of Microalloyed Steel,” *Weld. J.*, vol. 97, no. December, pp. 338s-352s,
39. Mohammadijoo M, Valloton J, Collins L, Henein H, Ivey DG (2018) “Characterization of martensite-austenite constituents and micro-hardness in intercritical reheated and coarse-grained heat affected zones of API X70 HSLA steel,” *Mater. Charact.*, vol. 142, no. May, pp. 321–331,

Tables

Table 1
Composition of X70 microalloyed steel and electrode (wt. %)

X70 Composition								
C	P	S	Mn	Si	N	V + Mo + Ti + Nb	Cu + Ni + Cr + Al + Ca	Fe
0.04	0.01	0.003	1.32	0.28	0.007	0.34	0.63	97.37
Electrode and cold-wire composition (BA-S2Mo)								
C	P	S	Mn	Si	Mo	Ni	Cr	Cu
0.1	0.007	0.01	1.04	0.1	0.56	0.02	0.03	0.03

Table 2
CWTSAW tests parameters and input levels

Symbol	**Process parameter**	**Notation**	**Unit**	**Level 1**	**Level 2**	**Level 3**	**Level 4**
A	Cold wire feed electrode	CWFS	mm/s	16.9	25.4	33.9	42.3
B	Heat input of lead electrode	HIL	kJ/mm	1.6	1.8	-	-
C	Heat input of trail electrode	HIT	kJ/mm	1.3	1.5	-	-
D	Voltage of lead electrode	VL	V	33	36	-	-
E	Voltage of lead electrode	VT	V	34	37	-	-
F	Travel speed	TS	mm/s	21.2	23.3	-	-
G	Bevel design	BD	mm^2	12	25	-	-

Table 3
L16 orthogonal array based on Taguchi analysis

Test no.	A(CWFS)	B(HIL)	C(HIT)	D(VL)	E(VT)	F(TS)	G(BD)
	(mm/s)	(kJ/mm)	(kJ/mm)	(V)	(V)	(mm/s)	(mm^2)
1	16.9	1.6	1.3	33	34	21.2	12
2	16.9	1.6	1.3	33	34	23.3	25
3	16.9	1.8	1.5	36	37	21.2	12
4	16.9	1.8	1.5	36	37	23.3	25
5	25.4	1.6	1.3	36	37	21.2	12
6	25.4	1.6	1.3	36	37	23.3	25
7	25.4	1.8	1.5	33	34	21.2	12
8	25.4	1.8	1.5	33	34	23.3	25
9	33.9	1.6	1.5	33	37	21.2	25
10	33.9	1.6	1.5	33	37	23.3	12
11	33.9	1.8	1.3	36	34	21.2	25
12	33.9	1.8	1.3	36	34	23.3	12
13	42.3	1.6	1.5	36	34	21.2	25
14	42.3	1.6	1.5	36	34	23.3	12
15	42.3	1.8	1.3	33	37	21.2	25
16	42.3	1.8	1.3	33	37	23.3	12

Table 4
Welding conditions for validation tests

Test no.	A(CWFS)	B(HIL)	C(HIT)	D(VL)	E(VT)	F(TS)	G(BD)
	(mm/s)	(kJ/mm)	(kJ/mm)	(V)	(V)	(mm/s)	(mm^2)
C1	25.4	2.0	1.4	36	34	21.2	25
C2	33.9	1.6	1.8	33	37	21.2	25
C3	29.6	1.8	1.4	33	38	21.2	25

Table 5
Measured weld characteristics

Trial No.	BW (mm)	HRA (mm)	BTA (°)	RA (mm^2)	CGHAZ area (mm^2)	CGHAZ hardness (HV0.5)	WM hardness (HV0.5)	PA (mm^2)	PD (mm)	$BW_{1/2}$ (mm)
1	14.0	5.0	123.5	51.3	22.1	215.9	230.0	123.2	11.6	12.0
2	13.4	4.2	127.8	39.5	27.5	**223.8**	233.2	139.7	13.0	12.1
3	15.3	4.4	125.2	47.5	24.2	220.6	234.7	139.1	12.3	12.7
4	14.1	3.6	130.7	35.0	26.0	220.1	**237.1**	161.0	13.7	**13.5**
5	15.1	4.0	127.0	45.4	20.8	216.2	233.7	119.4	10.9	12.1
6	14.7	3.9	135.7	36.8	24.4	222.3	232.0	142.6	12.2	13.1
7	13.2	**5.7**	111.8	**57.1**	26.1	216.6	232.9	139.2	13.3	12.0
8	12.4	5.2	113.5	47.9	**30.2**	215.1	234.4	**171.4**	**15.2**	13.4
9	14.7	3.5	124.0	37.4	27.4	212.9	229.7	142.9	13.2	12.2
10	13.3	4.9	121.7	49.2	23.8	215.0	235.4	135.4	12.8	12.3
11	14.7	3.2	**136.6**	31.9	27.8	208.9	225.8	143.4	13.1	12.5
12	14.4	4.9	119.8	52.9	23.0	215.4	228.8	132.8	12.1	12.2
13	**15.6**	4.0	133.2	43.1	25.7	213.8	232.7	136.6	12.4	11.7
14	12.8	5.5	112.1	52.3	23.1	219.9	236.1	134.4	12.8	11.9
15	13.5	3.5	136.0	31.2	27.8	215.6	234.3	142.3	13.1	11.8
16	13.3	4.9	119.6	47.1	22.2	209.7	230.5	134.7	12.5	12.4

Table 6
Calculated weld characteristics

Trial No.	1	2	3	4	5	6	7	8	9	10	11	12	13	14	15	16
AR	0.83	0.98	0.80	0.97	0.72	0.83	1.01	**1.22**	0.90	0.97	0.89	0.84	0.80	1.00	0.97	0.94
SPR	0.86	0.90	0.83	0.96	0.80	0.89	0.91	**1.08**	0.83	0.93	0.85	0.85	0.75	0.93	0.88	0.94
DIL	0.63	0.64	0.68	**0.69**	0.65	0.66	0.65	0.67	0.65	0.67	0.68	0.65	0.62	0.66	0.68	0.68

Table 7
P values for weld geometry results and CGHAZ and WM micro-hardness values

Characteristic	CWFS	HIL	HIT	VL	VT	TS	BD	Confidence level
BW	0.65	0.32	0.49	**0.012**	0.20	**0.023**	0.63	95%
HRA	**0.027**	0.70	**0.005**	**0.003**	**0.001**	**0.002**	**0.00**	
BTA	0.50	0.52	**0.021**	**0.05**	**0.05**	0.081	**0.004**	
RA	0.25	0.70	**0.023**	0.21	**0.006**	0.20	**0.00**	
CGHAZ area	0.31	**0.02**	**0.033**	**0.032**	0.10	0.28	**0.001**	
AR	0.59	**0.043**	**0.033**	**0.008**	0.10	**0.015**	0.11	
SPR	0.37	0.074	0.21	0.053	0.56	**0.008**	0.54	
DIL	0.76	**0.011**	0.37	0.44	**0.021**	0.23	1.00	
CGHAZ Hardness	**0.13**	0.28	0.70	0.42	0.86	**0.21**	0.83	75%
WM Hardness	**0.17**	0.65	**0.04**	0.95	**0.20**	**0.19**	0.77	

Table 8
Optimized levels of CWTSAW parameters

Criteria	Characteristics	CWFS (mm/s)	HIL (kJ/mm)	HIT (kJ/mm)	VL (V)	VT (V)	TS (mm/s)	BD (mm^2)
Higher-the-better	BW	33.9	1.6	1.3	36	37	21.2	25
	AR	25.4	1.8	1.5	33	34	23.3	25
	BTA	16.9	1.6	1.3	36	37	21.2	25
	SPR	25.4	1.8	1.5	33	34	23.3	25
Lower-the-better	RA	33.9	1.8	1.3	36	37	21.2	25
	CGHAZ area	16.9	1.6	1.3	36	37	23.3	12
	DIL	25.4	1.6	1.3	33	34	21.2	25
	HRA	33.9	1.6	1.3	36	37	21.2	25

Table 9
Welding condition of TSAW and CWTSAW

Process type	CWFS (mm/s)	HIL (kJ/mm)	HIT (kJ/mm)	VL (V)	VT (V)	TS (mm/s)	BD (mm^2)
TSAW	0	1.6	1.3	31	34	21.2	25
CWTSAW	16.9	1.6	1.3	31	34	21.2	25

Figures

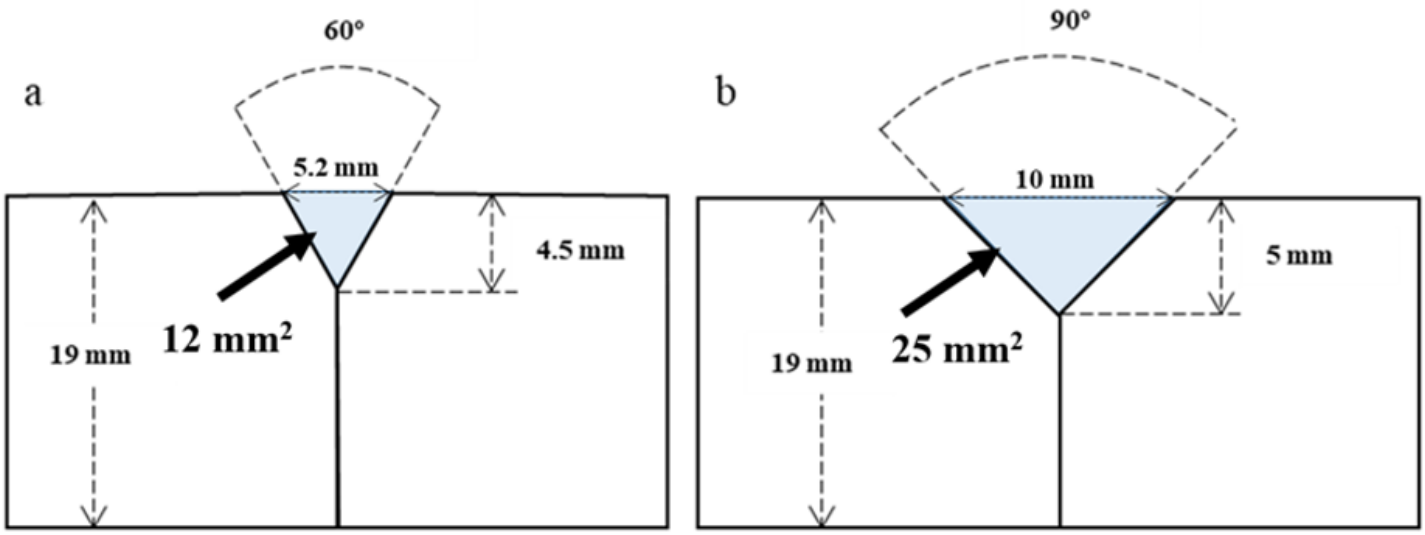

Figure 1

Schematic view of bevel specifications.

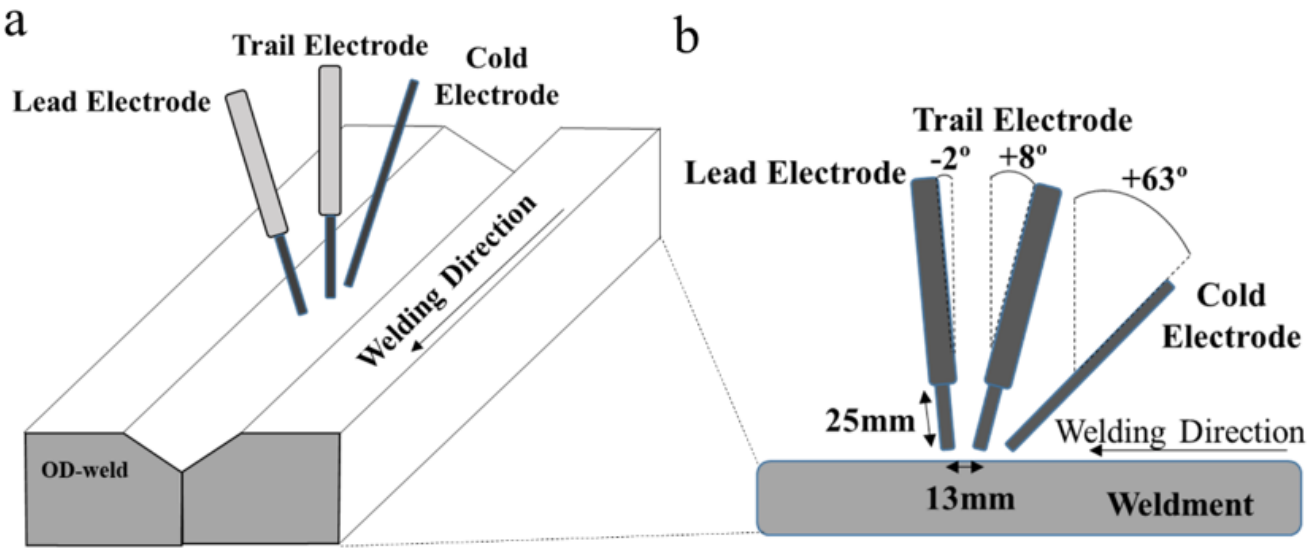

Figure 2

Setup for CWTSAW process: a) overview of welding set up, b) schematic view of fixed welding variables.

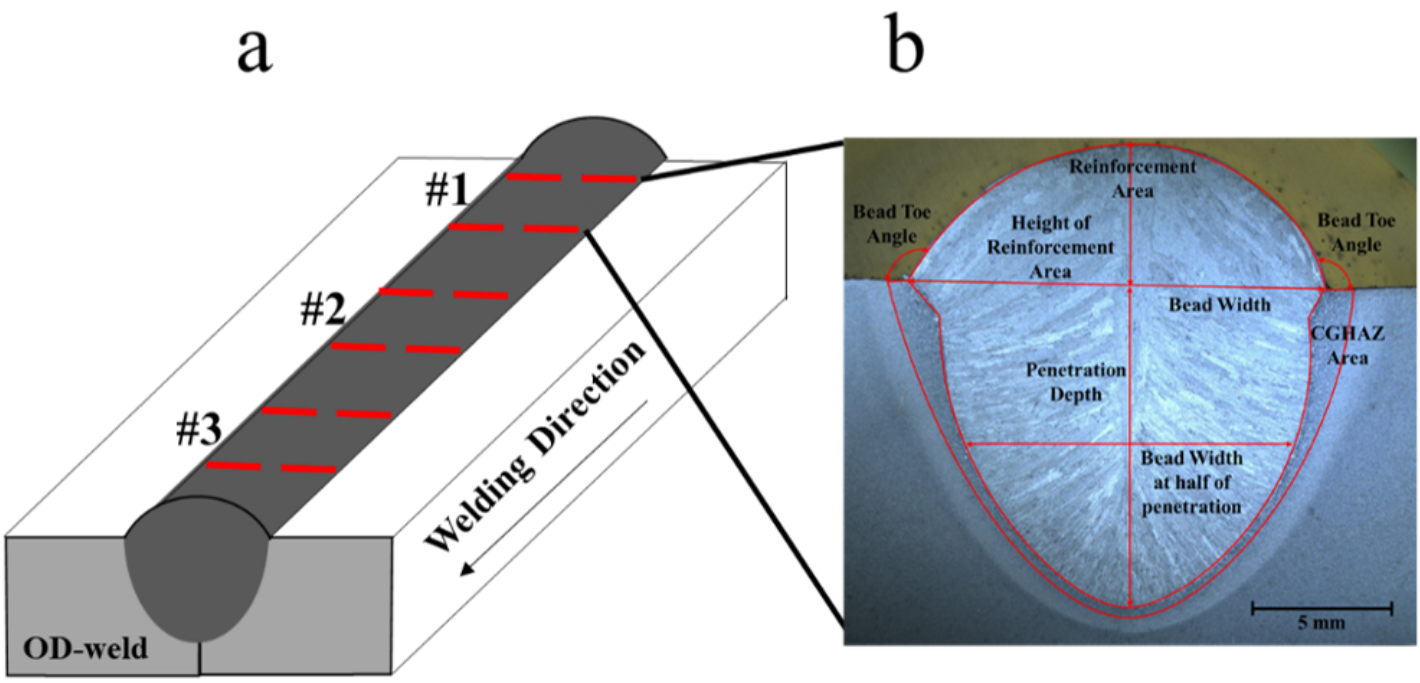

Figure 3

a) Schematic showing sectioning position of welds. b) Macrograph of Sample Test 1-1.

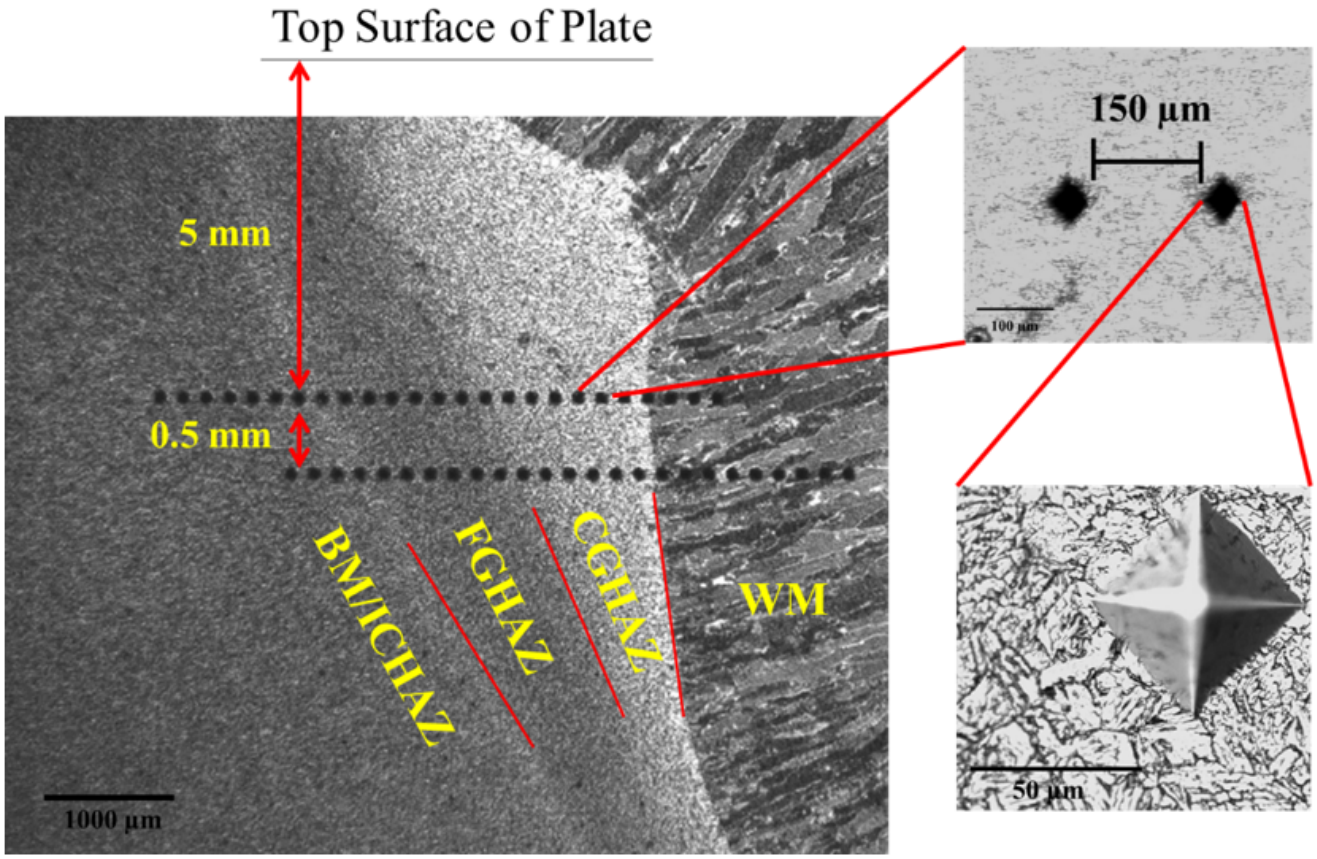

Figure 4

Schematic of the micro-hardness mapping along the HAZ and WM of Sample T1-1.

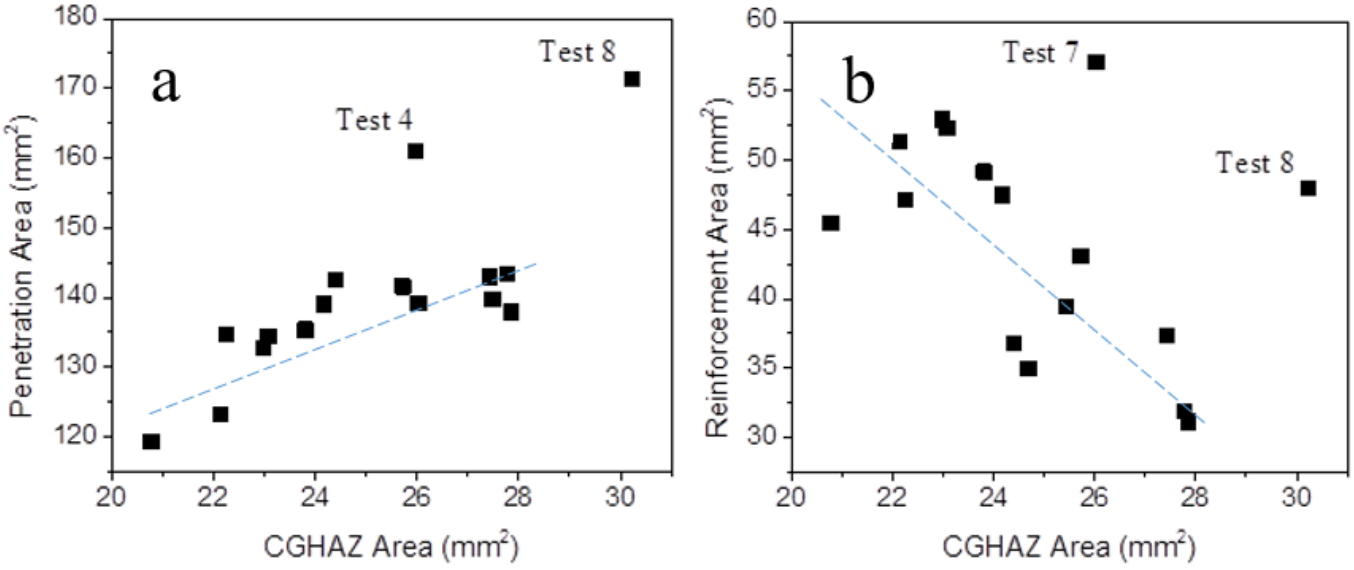

Figure 5

Plot of CGHAZ area vs. a) PA and b) RA.

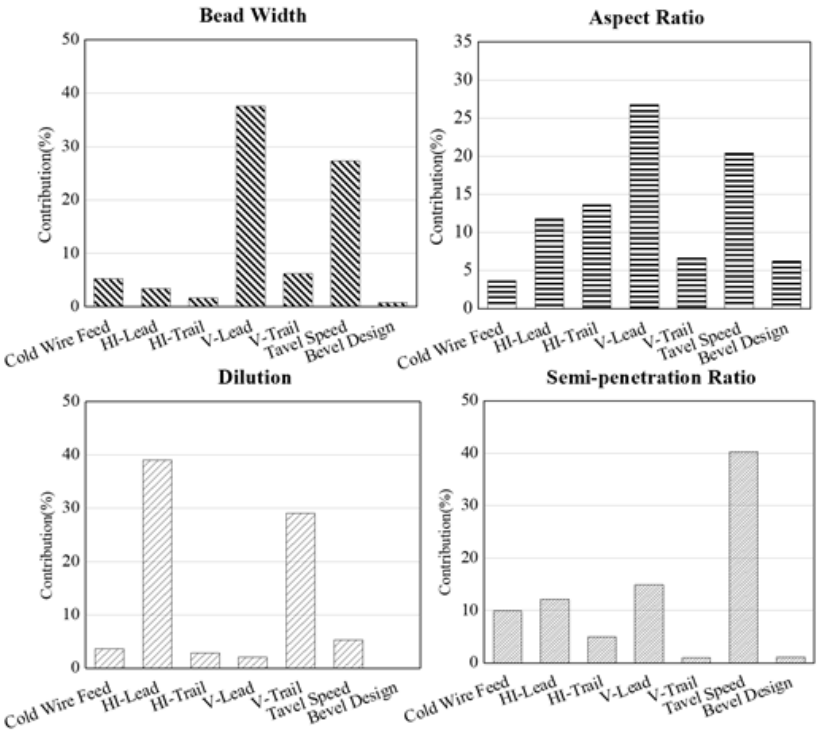

Figure 6

Effective contributions of CWTSAW process parameters for BW, AR, DIL, and SPR.

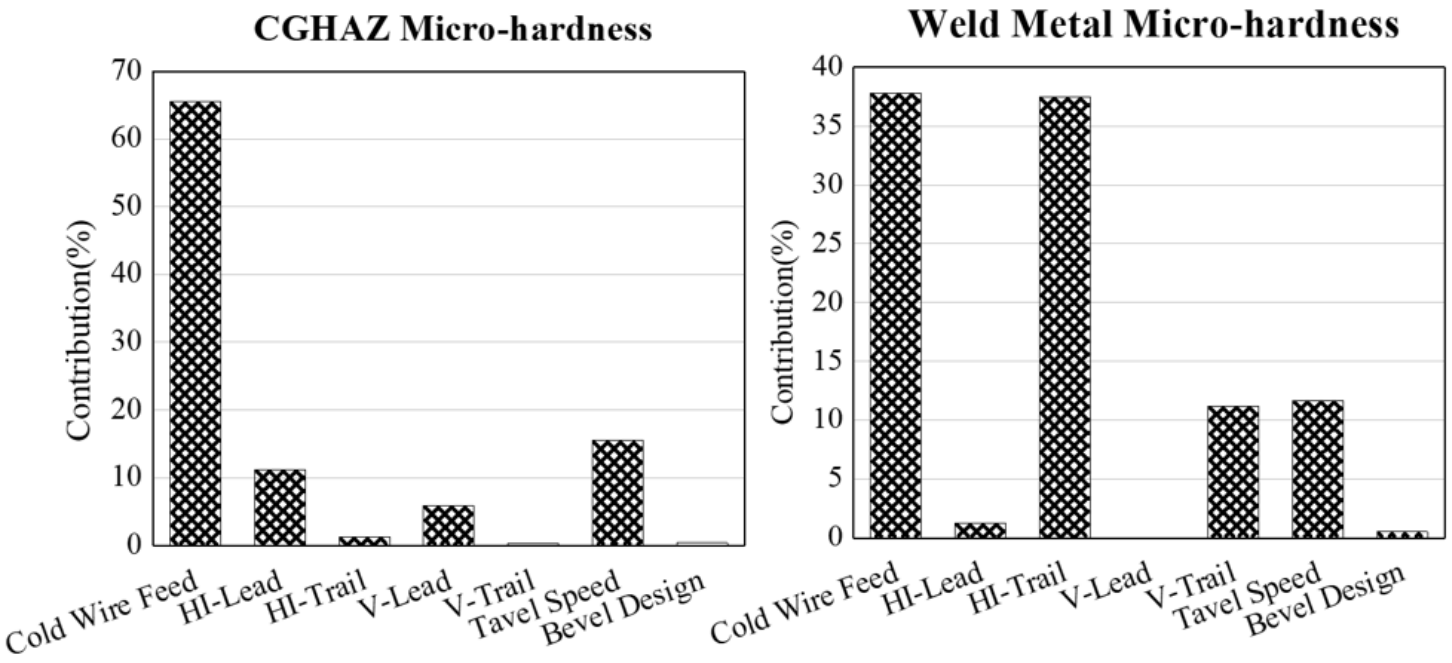

Figure 7

Effective contribution of CWTSAW process parameters for the WM and CGHAZ micro-hardness.

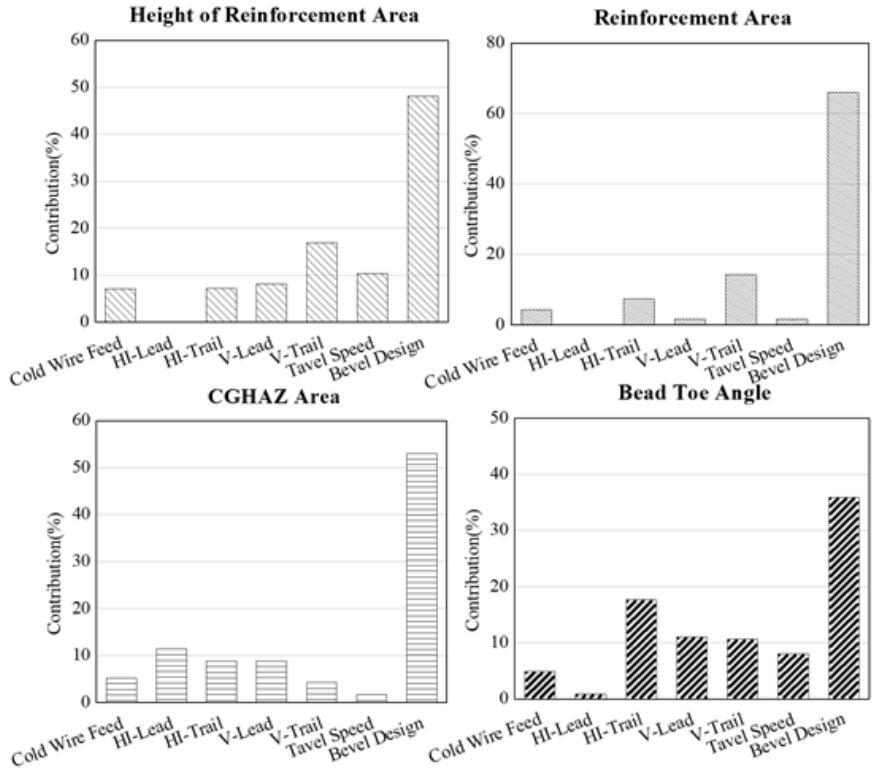

Figure 8

Effective contribution of CWTSAW process parameters for HRA, RA, CGHAZ area, and BTA.

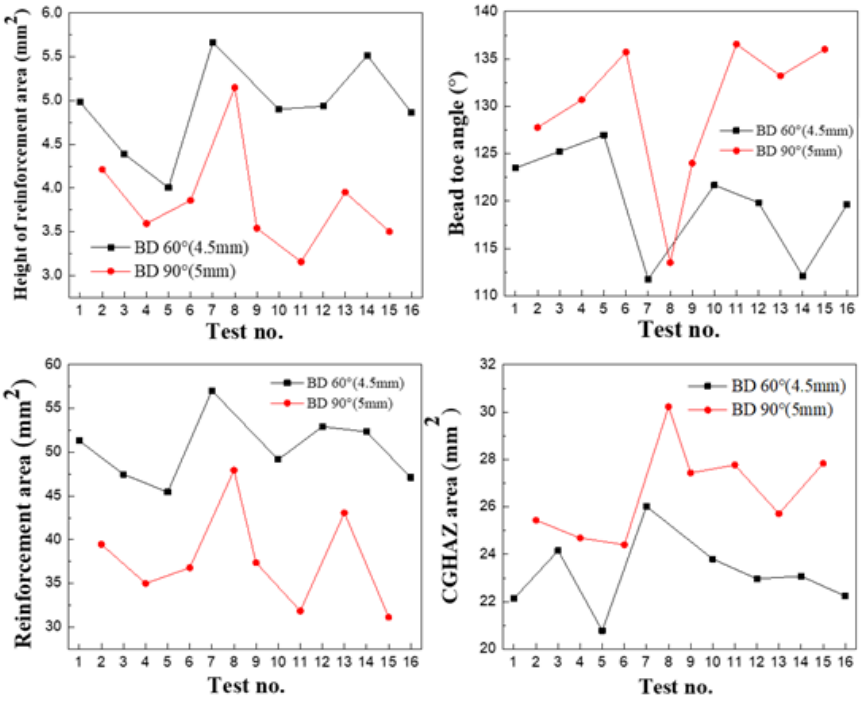

Figure 9

Measurements of RA, BTA, HRA and CGHAZ area for the two bevel specifications.

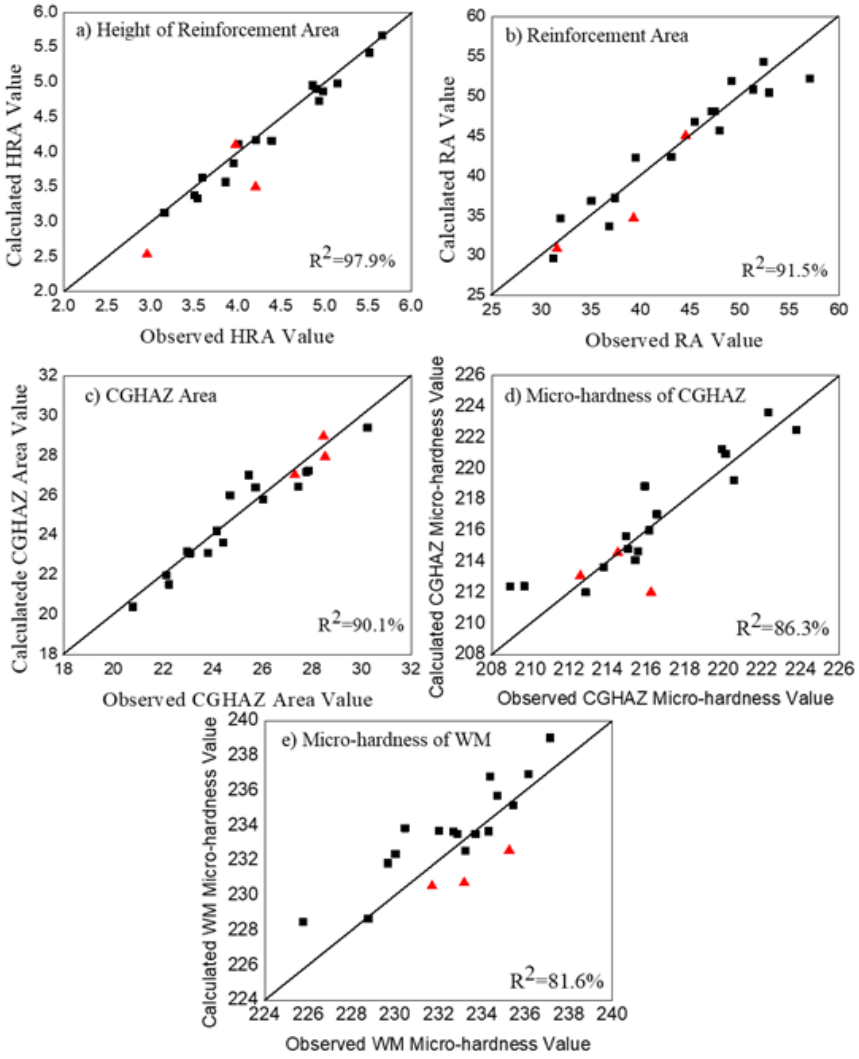

Figure 10

Observed and calculated values for the (a) HRA, (b) RA, (c) CGHAZ area, (d) micro-hardness of the CGHAZ, and (e) micro-hardness of the WM. Complementary tests results are also shown (triangles).

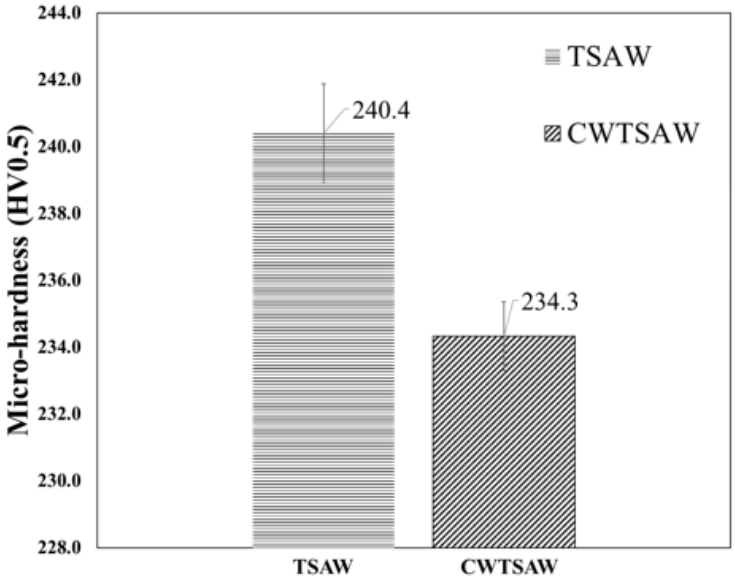

Figure 11

Average micro-hardness values in the CGHAZ for TSAW and CWTSAW.

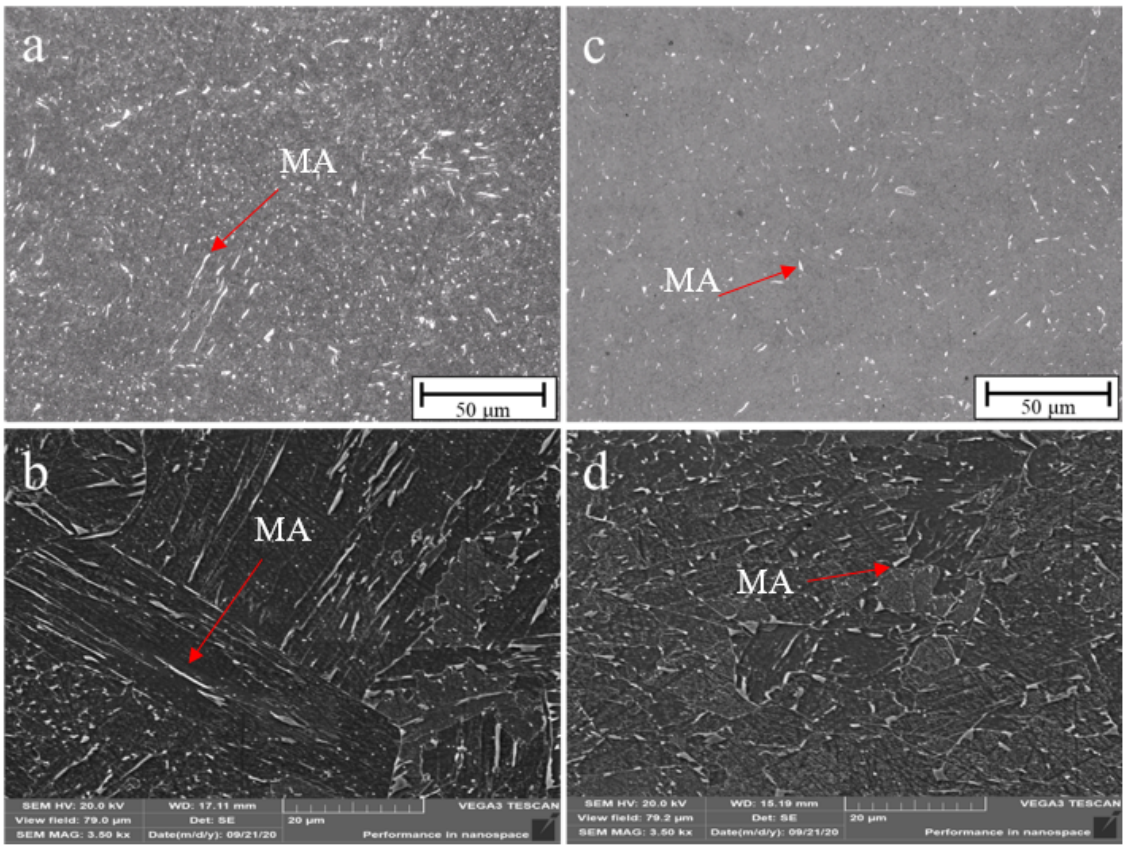

Figure 12

Weld samples fabricated by TSAW (a, b) and CWTSAW (c, d) showing MA constituents (shiny white phase) in the CGHAZ. Images a and c are optical micrographs, while images b and d are SEM SE micrographs.

Supplementary Files

This is a list of supplementary files associated with this preprint. Click to download.

- Appendix.docx